


# Efficient extreme-UV-to-extreme-UV conversion by four-wave mixing with intense near-IR pulses in highly charged ion plasmas

Hsu-hsin Chu<sup>1,\*</sup> and Jyhpyng Wang<sup>1,2,3</sup>

<sup>1</sup>*Department of Physics, National Central University, Zhongli 32001, Taiwan*

<sup>2</sup>*Institute of Atomic and Molecular Sciences, Academia Sinica, Taipei 10617, Taiwan*

<sup>3</sup>*Department of Physics, National Taiwan University, Taipei 10617, Taiwan*

 (Received 14 December 2017; revised manuscript received 27 April 2018; published 29 May 2018)

Nonlinear optics in the extreme-ultraviolet (EUV) has been limited by lack of transparent media and small conversion efficiency. To overcome this problem we explore the advantage of using multiply charged ion plasmas as the interacting media between EUV and intense near-infrared (NIR) pulses. Such media are transparent to EUV and can withstand intense NIR driving pulses without damage. We calculate the third-order nonlinear polarizabilities of Ar<sup>2+</sup> and Ar<sup>3+</sup> ions for EUV and NIR four-wave mixing by using the well-proven Cowan code and find that the EUV-to-EUV conversion efficiency as high as 26% can be expected for practical experimental configurations using multi-terawatt NIR lasers. Such a high efficiency is possible because the driving pulse intensity can be scaled up to several orders of magnitude higher than in conventional nonlinear media, and the group-velocity and phase mismatch are insignificant at the experimental plasma densities. This effective scheme of wave mixing can be utilized for ultrafast EUV waveform measurement and control as well as wavelength conversion.

DOI: [10.1103/PhysRevA.97.053840](https://doi.org/10.1103/PhysRevA.97.053840)

## I. INTRODUCTION

In the past few decades, the development of nonlinear optics has made a tremendous impact in many laser-related fields, such as laser spectroscopy, nonlinear microscopy, optical communication, material processing, quantum optics, terahertz radiation, ultrafast optics, high-field physics, etc. Limited by the transmittance of materials and laser sources, the spectral range of nonlinear optics has been largely confined to wavelengths longer than 200 nm. Recently, advancements in the ultrafast coherent extreme-ultraviolet (EUV) or x-ray sources, such as high-harmonic generation [1–3], EUV or x-ray lasers [4–7], and x-ray free-electron lasers [8–10], has greatly extended the capability of photoelectron spectroscopy [11], holographic microscopy [12,13], and coherent diffraction imaging [14–16] and opened new frontiers in attosecond sciences [1,17,18]. These coherent light sources not only can provide nanometer imaging resolutions, but also can excite or probe deep into the atomic core levels, which features element selectivity and chemical shift beyond the reach of conventional spectroscopy [19–21]. Nonlinear optics in the EUV spectral range can be anticipated to bring in a new wave of advancements in EUV lasers and optics.

Since the first demonstration of the third-harmonic generation of the vacuum-ultraviolet (VUV) (6–10 eV) in the mixture of Cd vapor and Ar gas [22], nonlinear wave mixing of VUV radiation in gases has been studied in different atoms with various experimental configurations [23–29]. Recently, narrow-band four-wave mixing (FWM) of EUV (~17 eV) and near-infrared (NIR) photons have been demonstrated [30]. In

this experiment, a broadband EUV attosecond pulse train was mixed with an intense NIR pulse in Ne atoms. Efficient narrow-band EUV emissions were observed at near-resonant FWM transitions. A similar experiment was done using Ar atoms with a noncollinear configuration [31], in which the output FWM waves were separated from the incident EUV wave in different directions. However, the photon energy range was still less than 20 eV. It is difficult to push the nonlinear interaction to shorter wavelengths with good conversion efficiency because most materials absorb EUV strongly. The EUV photon will be absorbed due to photoionization if its photon energy is larger than the material ionization potential. For example, four-wave mixing of EUV (~45 eV) and visible light was demonstrated on SiO<sub>2</sub> crystals, where the incident visible light was scattered by a transient grating induced by the interference of two intense EUV pulses [32]. The scattered wave in the visible is the four-wave-mixing output. The conversion efficiency is only about  $1.5 \times 10^{-7}$  because the nonlinear interaction is limited to the crystal surface owing to strong absorption in the bulk.

In this paper, we study the advantage of using highly charged ion plasma produced in a gas jet as the interacting medium for EUV-NIR mixing. The front edge of the intense NIR pulse ionizes the gas atoms into a highly charged ion plasma through strong field ionization [33–35], and the nonlinear response of the remaining bound electrons in the ions facilitates the mixing of EUV and NIR pulses. If the ionization potentials of the remaining bound electrons are larger than the EUV photon energy, photoionization will not occur and absorption of the EUV wave becomes negligible, thus the nonlinear interaction can be extended to shorter wavelengths. Since the third-order nonlinearity is the dominant nonlinear response for such an isotropic system, we focus on the four-wave mixing of one EUV photon (14–55 nm) plus two NIR photons

\*[hhchu@ncu.edu.tw](mailto:hhchu@ncu.edu.tw)

(810 nm) to a second EUV photon. We calculate the third-order nonlinear polarizabilities of  $\text{Ar}^{2+}$  and  $\text{Ar}^{3+}$  ions using Cowan's atomic structure code [36] and the Wigner-Eckart theorem. The calculated polarizabilities range from  $10^{-65}$  to  $10^{-60} \text{ C m}^4/\text{V}^3$ . For a  $1 \mu\text{J}$  EUV pulse (47.6 nm) and a 16.5 mJ NIR (810 nm) pulse mixing in a 2-mm-long Ar gas jet, the expected 42.6 nm four-wave mixing output is about 264 nJ, corresponding to an EUV-to-EUV conversion efficiency of 26%.

A highly desirable potential application of this EUV mixing scheme is the control and measurement of an ultrafast EUV waveform. For waveform control, spectral programming using a spatial light modulator in a pulse stretcher or compressor [37] or using an acousto-optic programmable dispersive filter [38] is limited by EUV absorption. Similarly, waveform measurement methods based on nonlinear optics are not applicable to EUV due to lack of transparent nonlinear media [39–41]. Several techniques based on laser-assisted photoelectric effects were developed to characterize the EUV waveform, such as frequency-resolved optical gating for complete reconstruction of attosecond bursts (FROG CRAB) [42,43] and resolution of attosecond beating by interference of two-photon transitions (RABBITT) [44,45]. In these techniques time-of-flight electron spectrometers are employed to measure the energy of photoelectrons coming from rare gases ionized by the EUV pulse when it overlaps a reference laser pulse. The photoelectron spectrum as a function of the delay between the two pulses is used to reconstruct the EUV waveform. However, delay scanning and data accumulation are required in these methods, thus the measurement cannot be done on a shot-to-shot basis.

Alternatively, an all-optical method based on spatially encoded transmission gating for measuring EUV waveforms has been developed [46]. In this method, a cross-propagating intense NIR gate pulse ionizes the EUV absorbing  $\text{H}_2$  molecules into nonabsorbing protons and creates a time sweep of transmission encoded spatially across the EUV pulse. The EUV temporal intensity profile is then retrieved from the lopsided spatial profile of the transmitted pulse. The method is all optical, and no data accumulation or shape assumption is needed. But only the intensity profile (without phase information) is measured. FWM with a known NIR waveform makes retrieving the complete EUV waveform possible. Since the NIR gate pulse can be characterized by well-established methods [39–41], the FWM spectrum as a function of the relative delay between the EUV pulse and the NIR pulse serves as a cross-correlation frequency-resolved optical gating (XFROG) trace, from which the EUV waveform can be retrieved directly by functional differentiation [47] or using the iterative XFROG algorithm [48]. Furthermore, as will be discussed in Sec. V, since the technology for NIR waveform synthesis has been well developed [38,49], such high-efficiency FWM can also be used for EUV temporal waveform control or wavelength conversion.

## II. CALCULATION OF THE THIRD-ORDER NONLINEAR POLARIZABILITY

Consider the mixing of three waves with angular frequencies  $\omega_p$ ,  $\omega_q$ , and  $\omega_r$ , respectively to generate an output wave with angular frequency  $\omega_\sigma = \omega_p + \omega_q + \omega_r$ . The third-order polarizability of an atom or ion is

$$\alpha_{kjih}^{(3)} = \frac{P_I}{\hbar^3} \sum_{vnm} \left[ \frac{\mu_{gv}^k \mu_{vn}^j \mu_{nm}^i \mu_{mg}^h}{(\omega_{vg} - \omega_r - \omega_q - \omega_p - i\gamma_{vg})(\omega_{ng} - \omega_q - \omega_p - i\gamma_{ng})(\omega_{mg} - \omega_p - i\gamma_{mg})} \right. \\ + \frac{\mu_{gv}^j \mu_{vn}^k \mu_{nm}^i \mu_{mg}^h}{(\omega_{vg} + \omega_r + i\gamma_{vg})(\omega_{ng} - \omega_q - \omega_p - i\gamma_{ng})(\omega_{mg} - \omega_p - i\gamma_{mg})} \\ + \frac{\mu_{gv}^j \mu_{vn}^i \mu_{nm}^k \mu_{mg}^h}{(\omega_{vg} + \omega_r + i\gamma_{vg})(\omega_{ng} + \omega_r + \omega_q + i\gamma_{ng})(\omega_{mg} - \omega_p - i\gamma_{mg})} \\ \left. + \frac{\mu_{gv}^j \mu_{vn}^i \mu_{nm}^h \mu_{mg}^k}{(\omega_{vg} + \omega_r + i\gamma_{vg})(\omega_{ng} + \omega_r + \omega_q + i\gamma_{ng})(\omega_{mg} + \omega_r + \omega_q + \omega_p + i\gamma_{mg})} \right], \quad (1)$$

where  $P_I$  is the intrinsic permutation operator of frequencies  $\omega_p$ ,  $\omega_q$ , and  $\omega_r$  [50]. The indices  $g$ ,  $m$ ,  $n$ , and  $v$  represent the ground state  $|g\rangle$ , first excitation state  $|m\rangle$ , second excitation state  $|n\rangle$ , and third excitation state  $|v\rangle$ , respectively.  $\mu_{nm}^i$  is the matrix element of electric dipole operator that  $\mu_{nm}^i = \langle n | \mu_i | m \rangle = -e \langle n | r_i | m \rangle$ .  $\omega_{nm} = \Delta E_{nm} / \hbar$ , where  $\Delta E_{nm}$  is the energy difference between states  $|n\rangle$  and  $|m\rangle$ .  $\gamma_{nm}$  equals  $(\Gamma_n + \Gamma_m) / 2$ , where  $\Gamma_n$  and  $\Gamma_m$  are the population decay rates of  $|n\rangle$  and  $|m\rangle$ .

Assume all optical waves are polarized in the  $z$  direction and their frequencies are not close to resonances. The decay rates can be neglected. Then the polarizability can be simplified to

$$\alpha_{zzzz}^{(3)} = \frac{P_I}{\hbar^3} \sum_{vnm} \mu_{gv}^z \mu_{vn}^z \mu_{nm}^z \mu_{mg}^z \left[ \frac{1}{(\omega_{vg} - \omega_r - \omega_q - \omega_p)(\omega_{ng} - \omega_q - \omega_p)(\omega_{mg} - \omega_p)} \right. \\ + \frac{1}{(\omega_{vg} + \omega_r)(\omega_{ng} - \omega_q - \omega_p)(\omega_{mg} - \omega_p)} + \frac{1}{(\omega_{vg} + \omega_r)(\omega_{ng} + \omega_r + \omega_q)(\omega_{mg} - \omega_p)} \\ \left. + \frac{1}{(\omega_{vg} + \omega_r)(\omega_{ng} + \omega_r + \omega_q)(\omega_{mg} + \omega_r + \omega_q + \omega_p)} \right] = \sum_{vnm} \alpha_{vnm}^{(3)}. \quad (2)$$

TABLE I. Electron configurations of the  $\text{Ar}^{2+}$  excitation states included in the calculation. The common part  $[\text{Ne}] 3s^2$  is not listed.

First	Second	Third
$3p^3 4s^1$	$3p^3 4p^1$	$3p^3 4s^1$
$3p^3 5s^1$	$3p^3 5p^1$	$3p^3 5s^1$
$3p^3 6s^1$	$3p^3 6p^1$	$3p^3 6s^1$
$3p^3 3d^1$	$3p^3 7p^1$	$3p^3 3d^1$
$3p^3 4d^1$	$3p^2 3d^2$	$3p^3 4d^1$
$3p^3 5d^1$	$3p^2 3d^1 4d^1$	$3p^3 5d^1$
$3p^3 6d^1$	$3p^2 4s^1 3d^1$	$3p^3 6d^1$
	$3p^2 4s^1 5s^1$	
	$3p^2 4s^1 6s^1$	

By using Cowan's atomic structure code [36], the energy differences  $\Delta E_{nm}$  and reduced dipole matrix elements  $\langle \alpha j \| \mathbf{r}_0^{(1)} \| \alpha' j' \rangle$  can be calculated, where  $\alpha$  and  $\alpha'$  represent the quantum numbers other than angular momentum,  $j$  and  $j'$  are angular momentum quantum numbers, and  $\mathbf{r}_0^{(1)} = z$  is the 0th-component of the irreducible tensor operator  $\mathbf{r}^{(1)}$  of rank 1. Then the dipole matrix elements can be calculated using the Wigner-Eckart theorem [51]:

$$\begin{aligned} \langle \alpha j m | \mu_z | \alpha' j' m' \rangle &= -e \langle \alpha j m | \mathbf{r}_0^{(1)} | \alpha' j' m' \rangle \\ &= -e (-1)^{j-m} \begin{pmatrix} j & 1 & j' \\ -m & 0 & m' \end{pmatrix} \langle \alpha j \| \mathbf{r}_0^{(1)} \| \alpha' j' \rangle, \end{aligned} \quad (3)$$

where  $m$  and  $m'$  are magnetic quantum numbers, and  $\begin{pmatrix} j & 1 & j' \\ -m & 0 & m' \end{pmatrix}$  is the Wigner 3- $j$  symbol. With  $\Delta E_{nm}$  and dipole matrix elements the nonlinear polarizability  $\alpha_{zzz}^{(3)}$  can be evaluated.

In the calculation of nonlinear polarizability the NIR photon energy is fixed at 1.53 eV, corresponding to the 810 nm output wavelength of our Ti:sapphire laser [52]. For the  $\text{Ar}^{2+}$  ion the required photon energy to ionize its outmost electron is 72.07 eV.<sup>1</sup> Therefore, such ion species can be used for the interaction of EUV photons with wavelengths longer than 17.2 nm. The ground electron configuration of  $\text{Ar}^{2+}$  is  $[\text{Ne}] 3s^2 3p^4$ , which includes five  $LS$ -split subshells  $^3P_2$ ,  $^3P_1$ ,  $^3P_0$ ,  $^1D_2$ , and  $^1S_0$ . The energy of these five states are calculated using Cowan's code. Since the ions are prepared by a gas jet ionized by a femtosecond NIR pulse, the temperature of the gas should be less than room temperature due to rapid expansion. Furthermore, the ionization and wave-mixing process will be done within the femtosecond NIR and EUV pulse durations (e.g., about 30 fs for the proposed experiment

in Sec. IV). The rescattering of the ionized electron under such a low-ionization-potential and high-laser-intensity condition within such a short timescale is not significant [53]. Therefore, excitation of the residual bound electrons due to recollision can be neglected. We assume the ground state population obeys Boltzmann distribution under room temperature. About 99.8% of the population stays in the lowest-energy state  $^3P_2$ , and only 0.2% population stays in the second lowest state  $^3P_1$ . Therefore, we calculate the nonlinear polarizability using  $^3P_2$  as the ground state. The contribution of other subshells is negligible. The electron configurations of the excited states included in our calculation are listed in Table I, and the energy diagram is shown in Fig. 1.

Combining the reduced dipole matrix elements and the Wigner-Eckart theorem, the dipole matrix elements are obtained. Then the third-order nonlinear polarizability  $\alpha^{(3)}$  is calculated as a function of the input EUV wavelength. The absolute value of  $\alpha^{(3)}$  is shown in Fig. 2. It ranges from  $10^{-65}$  to  $10^{-60} \text{ C m}^4/\text{V}^3$  for wavelengths between 18 and 55 nm. In this calculation, about 160 000 transitions are included, which consist of the majority of bound states with energies lower than the ionization energy of the rest of electrons in the  $\text{Ar}^{2+}$  ion.

For the  $\text{Ar}^{3+}$  ion the required photon energy to ionize its outmost electron is 89.12 eV. Such ion species can be used for the interaction of EUV photons with wavelengths longer than 13.9 nm. The ground electron configuration is  $[\text{Ne}] 3s^2 3p^3$ , which also includes five  $LS$ -split subshells:  $^4S_{3/2}$ ,  $^2D_{3/2}$ ,  $^2D_{5/2}$ ,  $^2P_{1/2}$ , and  $^2P_{3/2}$ . Assume the ground state population obeys a Boltzmann distribution under room temperature. Almost all of the population ( $> 99.99\%$ ) stays in the lowest-energy state  $^4S_{3/2}$ . Therefore, we choose  $^4S_{3/2}$  as the ground state for our calculation. The electron configurations of the included excitation states are listed in Table II, and the energy diagram is shown in Fig. 3. The absolute value of  $\alpha^{(3)}$  is also shown in Fig. 2. It ranges from  $10^{-65}$  to  $10^{-61} \text{ C m}^4/\text{V}^3$  for wavelengths between 14 and 55 nm. In this calculation, about 200 000 combinations of the transitions are included. Far-from-resonance transitions not included in the calculation contribute less than 1% of the nonlinear polarizability.

Figure 2 shows that near-resonant transitions result in large nonlinear polarizability, such as the local maximums of the  $\text{Ar}^{2+}$  at 21.9 nm and 47.6 nm, and that of  $\text{Ar}^{3+}$  at 18.8 nm. For off-resonant transitions, the angular frequency differences ( $\Delta\omega$ ) in the dominators in Eq. (2) are on the order of  $10^{16} \text{ Hz}$ . For near-resonant transitions,  $\Delta\omega$  are  $10^{13}$ - $10^{14} \text{ Hz}$ . Therefore, their contributions to the nonlinear polarizability are greatly enhanced. Yet these transitions are not so resonant as to cause absorption. This is verified by calculation with Cowan's code that the decay rates  $[\gamma_{nm}$  in Eq. (1)] are  $10^7$ - $10^{11} \text{ sec}^{-1}$ . Therefore, these  $\gamma_{nm}$  can be neglected, as stated in Sec. II.

### III. CALCULATION OF THE ABSOLUTE YIELD

Once the nonlinear polarizability is obtained, the absolute yield of the FWM process can be calculated by solving the system of third-order nonlinear wave equations. Assume the input NIR field, input EUV field, and output FWM field have

<sup>1</sup>In general, ionization potential of the third electron of Ar atom is 40.74 eV, which is the energy difference between the state of  $[\text{Ne}] 3s^2 3p^4 + 2 \text{ free } e^-$  and the state of  $[\text{Ne}] 3s^2 3p^3 + 3 \text{ free } e^-$ . However, the condition we considered is the photoionization of the outmost electron of a preionized  $\text{Ar}^{2+}$  ion. Following Cowan's code, the energy difference between the state of  $[\text{Ne}] 3s^2 3p^4$  and the state of  $[\text{Ne}] 3s^2 3p^3 + 1 \text{ free } e^-$  is 72.07 eV, corresponding to a wavelength of 17.2 nm.

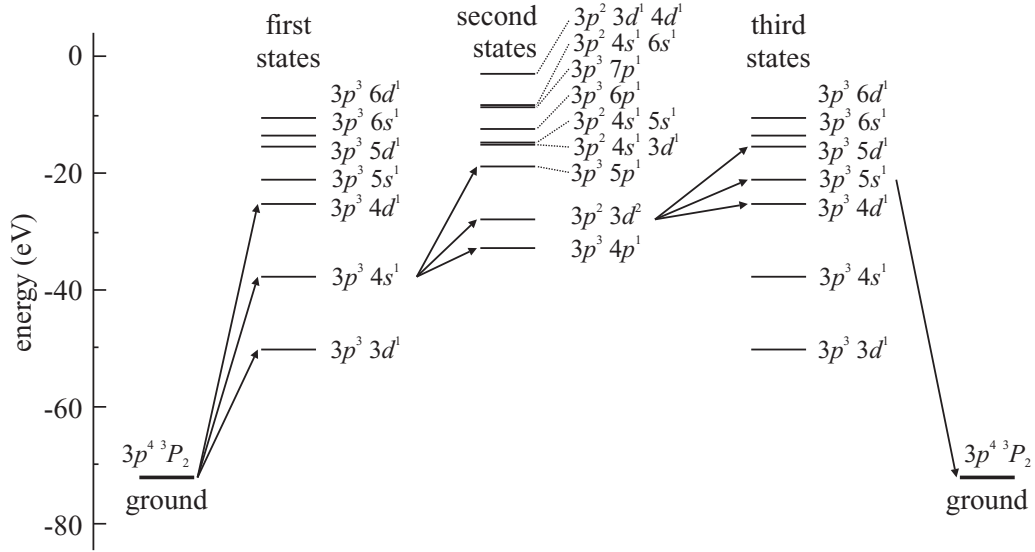


FIG. 1. Energy diagram of  $\text{Ar}^{2+}$  ion. The ground state is  $3p^4 \ ^3P_2$ . The fine structures of the excited states are not shown but are included in our calculation.

a slowly varying amplitude in  $z$ ,

$$E_{\text{NIR}}(z, t) = E_{\text{NIR}}(z) e^{i(k_{\text{NIR}}z - \omega_{\text{NIR}}t)} + \text{c.c.} \quad (4a)$$

$$E_{\text{EUV}}(z, t) = E_{\text{EUV}}(z) e^{i(k_{\text{EUV}}z - \omega_{\text{EUV}}t)} + \text{c.c.} \quad (4b)$$

$$E_{\text{out}}(z, t) = E_{\text{out}}(z) e^{i(k_{\text{out}}z - \omega_{\text{out}}t)} + \text{c.c.}, \quad (4c)$$

where  $\omega_{\text{NIR}}$ ,  $\omega_{\text{EUV}}$ , and  $\omega_{\text{out}}$  are the angular frequencies of the input NIR field, input EUV field, and output FWM field, respectively,  $k_{\text{NIR}}$ ,  $k_{\text{EUV}}$ , and  $k_{\text{out}}$  are the wave numbers of the input NIR field, input EUV field, and output FWM field, respectively, and c.c. represents the complex conjugate. The

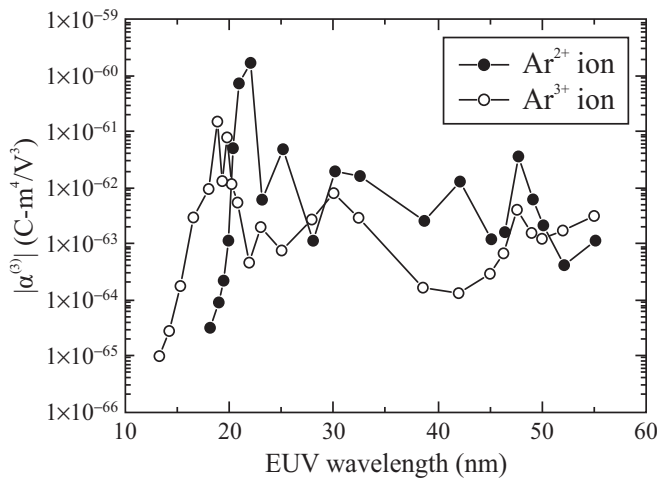


FIG. 2. The absolute values of the third-order nonlinear polarizabilities  $\alpha^{(3)}$  of  $\text{Ar}^{2+}$  (filled circle) and  $\text{Ar}^{3+}$  (open circle) for the four-wave mixing of 1 EUV photon plus 2 NIR photons to a second EUV photon as functions of the input EUV wavelength.

system of third-order nonlinear wave equations are

$$\frac{dE_{\text{NIR}}(z)}{dz} = \frac{3i\omega_{\text{NIR}}}{c n_{\text{NIR}}} \chi^{(3)} E_{\text{NIR}}^*(z) E_{\text{EUV}}^*(z) E_{\text{out}}(z) e^{-i\Delta kz} \quad (5a)$$

$$\frac{dE_{\text{EUV}}(z)}{dz} = \frac{3i\omega_{\text{EUV}}}{2c n_{\text{EUV}}} \chi^{(3)} E_{\text{out}}(z) E_{\text{NIR}}^*(z)^2 e^{-i\Delta kz} \quad (5b)$$

$$\frac{dE_{\text{out}}(z)}{dz} = \frac{3i\omega_{\text{out}}}{2c n_{\text{out}}} \chi^{(3)} E_{\text{NIR}}(z)^2 E_{\text{EUV}}(z) e^{i\Delta kz}, \quad (5c)$$

where  $n_{\text{NIR}}$ ,  $n_{\text{EUV}}$ , and  $n_{\text{out}}$  are the refractive indices of the input NIR field, input EUV field, and output FWM field, respectively,  $\chi^{(3)} = N_{\text{ion}}\alpha^{(3)}/\epsilon_0$  is the third-order nonlinear susceptibility in dilute medium,  $N_{\text{ion}}$  is the ion density,  $\alpha^{(3)}$  is the third-order nonlinear polarizability calculated in last section, and  $\Delta k = 2k_{\text{NIR}} + k_{\text{EUV}} - k_{\text{out}}$  is the wave number mismatch due to plasma dispersion and Gouy phase shift.

In the FWM process if the depletion of input NIR field is insignificant, it can be treated as a constant, i.e.,  $E_{\text{NIR}}(z) = E_{\text{NIR}}$ . The boundary conditions of  $E_{\text{EUV}}(z)$  and  $E_{\text{out}}(z)$  are  $E_{\text{EUV}}(0) = E_0$  and  $E_{\text{out}}(0) = 0$ , respectively. In this case solutions of the input EUV field  $E_{\text{EUV}}(z)$  and the output FWM field  $E_{\text{out}}(z)$  are

$$E_{\text{EUV}}(z) = E_0 \left[ \cos(gz) + \frac{i\Delta k}{2g} \sin(gz) \right] e^{-i(\Delta k/2)z} \quad (6a)$$

$$E_{\text{out}}(z) = \frac{3i\omega_{\text{out}}}{2c n_{\text{out}}} \frac{\chi^{(3)}}{g} E_{\text{NIR}}^2 E_0 \sin(gz) e^{i(\Delta k/2)z}, \quad (6b)$$

where

$$g = \sqrt{\frac{1}{4}\Delta k^2 + \frac{9\omega_{\text{EUV}}\omega_{\text{out}}}{16\epsilon_0^2 c^4 n_{\text{NIR}}^2 n_{\text{EUV}} n_{\text{out}}} \chi^{(3)2} J_{\text{NIR}}^2}, \quad (7)$$

and

$$I_{\text{NIR}} = 2\epsilon_0 n_{\text{NIR}} c |E_{\text{NIR}}|^2 \quad (8)$$

is the NIR intensity.

The wave-number mismatch  $\Delta k$  is the sum of the Ar plasma dispersion ( $\Delta k_{\text{plasma}}$ ) and the Gouy phase shift ( $\Delta k_{\text{Gouy}}$ ) ( $\Delta k = \Delta k_{\text{plasma}} + \Delta k_{\text{Gouy}}$ ). For the plasma dispersion,

$$\Delta k_{\text{plasma}} = 2 \frac{\omega_{\text{NIR}}}{c} n_{\text{NIR}} + \frac{\omega_{\text{EUV}}}{c} n_{\text{EUV}} - \frac{\omega_{\text{out}}}{c} n_{\text{out}}. \quad (9)$$

The refractive indices  $n_{\text{NIR}}$ ,  $n_{\text{EUV}}$ , and  $n_{\text{out}}$  are determined by their angular frequencies:

$$n(\omega) = \sqrt{1 - \frac{N_e e^2}{\epsilon_0 m_e \omega^2}}, \quad (10)$$

where  $N_e$  is the electron density,  $e$  is the elementary charge, and  $m_e$  is the electron mass.

For the Gouy phase shift,

$$\Delta k_{\text{Gouy}} = \frac{1}{L} \left\{ 2 \left[ -2 \tan^{-1} \left( \frac{L}{2 b_{\text{NIR}}} \right) \right] + \left[ -2 \tan^{-1} \left( \frac{L}{2 b_{\text{EUV}}} \right) \right] - \left[ -2 \tan^{-1} \left( \frac{L}{2 b_{\text{out}}} \right) \right] \right\}, \quad (11)$$

where  $L$  is the total interaction length,  $b_{\text{NIR}} = \pi w_{0,\text{NIR}}^2 / \lambda_{\text{NIR}}$ ,  $b_{\text{EUV}} = \pi w_{0,\text{EUV}}^2 / \lambda_{\text{EUV}}$ , and  $b_{\text{out}} = \pi w_{0,\text{out}}^2 / \lambda_{\text{out}}$  are the confocal parameters of the NIR, EUV, and output beams, respectively. The  $w_{0,\text{NIR}}$  and  $w_{0,\text{EUV}}$  are the waist radius of the input NIR and EUV beam. The output FWM beam radius is set equal to the input EUV beam radius.

Finally, the input EUV intensity and output FWM intensity as functions of interaction length  $z$  are obtained:

$$I_{\text{EUV}}(z) = I_{\text{EUV}}(0) \times \left[ \cos^2(gz) + \frac{\Delta k^2}{4g^2} \sin^2(gz) \right] \quad (12a)$$

$$I_{\text{out}}(z) = \frac{9 \chi^{(3)2} \omega_{\text{out}}^2}{16 \epsilon_0^2 c^4 n_{\text{NIR}}^2 n_{\text{EUV}} n_{\text{out}}} \frac{1}{g^2} \times I_{\text{NIR}}^2 I_{\text{EUV}}(0) \sin^2(gz), \quad (12b)$$

where

$$I_{\text{EUV}}(0) = 2 \epsilon_0 n_{\text{EUV}} c |E_0|^2 \quad (13)$$

is the initial input EUV intensity.

#### IV. A CASE STUDY OF PRACTICAL EXPERIMENT

In recent experiments of high-harmonic generation, EUV pulses with a few tens of femtoseconds duration and a few microjoules energy are obtained [54–56]. In this section we study a practical experimental configuration for four-wave mixing of microjoule EUV pulse and millijoule NIR pulse using  $\text{Ar}^{2+}$  ions. The NIR wavelength is selected to be 810 nm, which is a typical wavelength of femtosecond Ti:sapphire lasers. The input EUV wavelength is 47.6 nm (17th harmonic of the NIR wave). The configuration is shown in Fig. 4. The input EUV beam and NIR beam are focused onto an Ar gas jet colinearly. The intense NIR pulse ionizes the Ar atoms to  $\text{Ar}^{2+}$  ions, then mixes with the EUV pulse by the nonlinear response of the electrons in the  $\text{Ar}^{2+}$  ions.

TABLE II. Electron configurations of the  $\text{Ar}^{3+}$  excitation states included in the calculation. The common part  $[\text{Ne}] 3s^2$  is not listed.

First	Second	Third
$3p^2 4s^1$	$3p^2 4p^1$	$3p^2 4s^1$
$3p^2 5s^1$	$3p^2 5p^1$	$3p^2 5s^1$
$3p^2 6s^1$	$3p^2 6p^1$	$3p^2 6s^1$
$3p^2 3d^1$	$3p^2 7p^1$	$3p^2 3d^1$
$3p^2 4d^1$	$3p^1 3d^2$	$3p^2 4d^1$
$3p^2 5d^1$	$3p^1 3d^1 4d^1$	$3p^2 5d^1$
$3p^2 6d^1$	$3p^1 3d^1 4s^1$	$3p^2 6d^1$
	$3p^1 4s^1 5s^1$	
	$3p^1 4s^1 6s^1$	

To evaluate the FWM yield, we assume both the input NIR and EUV pulses are three-dimensional transform-limited Gaussian pulses. Their intensity distributions at focal spots are

$$I_{\text{NIR}}(r,t) = \frac{2U_{\text{NIR}}}{\pi^{3/2} \tau_{\text{NIR}} w_{0,\text{NIR}}^2} \exp\left(-\frac{2r^2}{w_{0,\text{NIR}}^2}\right) \exp\left(-\frac{t^2}{\tau_{\text{NIR}}^2}\right) \quad (14)$$

and

$$I_{\text{EUV}}(r,t) = \frac{2U_{\text{EUV}}}{\pi^{3/2} \tau_{\text{EUV}} w_{0,\text{EUV}}^2} \times \exp\left(-\frac{2r^2}{w_{0,\text{EUV}}^2}\right) \exp\left(-\frac{t^2}{\tau_{\text{EUV}}^2}\right), \quad (15)$$

respectively, where  $U_{\text{NIR}} = 16.5$  mJ is the NIR (810 nm) pulse energy,  $U_{\text{EUV}} = 1$   $\mu\text{J}$  is the EUV (47.6 nm) pulse energy,  $\tau_{\text{NIR}} = 30$  fs is the NIR pulse duration,  $\tau_{\text{EUV}} = 20$  fs is the EUV pulse duration,  $w_{0,\text{NIR}} = 80$   $\mu\text{m}$  is the NIR waist radius, and  $w_{0,\text{EUV}} = 40$   $\mu\text{m}$  is the EUV waist radius. Therefore, the peak intensities of these two fields are  $I_{\text{NIR}}(0,0) = 3.1 \times 10^{15}$  W/cm<sup>2</sup> and  $I_{\text{EUV}}(0,0) = 1.1 \times 10^{12}$  W/cm<sup>2</sup>, respectively. The NIR beam size is chosen to be twice as the EUV beam size to ensure that the EUV pulse meets more uniform NIR intensity and ion density profiles.

The spectra of the input NIR and EUV pulses are

$$\tilde{E}_{\text{NIR}}(\omega) = \tilde{E}_{\text{NIR}} \exp\left[-\frac{(\omega - \omega_{\text{NIR},c})^2}{2\Delta\omega_{\text{NIR}}^2}\right] \quad (16)$$

and

$$\tilde{E}_{\text{EUV}}(\omega) = \tilde{E}_{\text{EUV}} \exp\left[-\frac{(\omega - \omega_{\text{EUV},c})^2}{2\Delta\omega_{\text{EUV}}^2}\right], \quad (17)$$

respectively, where  $\omega_{\text{NIR},c} = 2.33 \times 10^{15}$  Hz is the NIR central angular frequency,  $\omega_{\text{EUV},c} = 3.96 \times 10^{16}$  Hz is the EUV central angular frequency,  $\Delta\omega_{\text{NIR}} = 1/\tau_{\text{NIR}} = 3.33 \times 10^{13}$  Hz is the NIR bandwidth, and  $\Delta\omega_{\text{EUV}} = 1/\tau_{\text{EUV}} = 5 \times 10^{13}$  Hz is the EUV bandwidth. Since these bandwidths are comparable to the off-resonant frequencies ( $10^{13}$ – $10^{14}$  Hz) discussed in Sec. II, using a polarizability with fixed frequencies [ $\alpha^{(3)}(\omega_{\text{NIR},c}, \omega_{\text{EUV},c}, \omega_{\text{out}})$ ] may not be sufficiently accurate. For better accuracy, we take nine sample points of their spectra



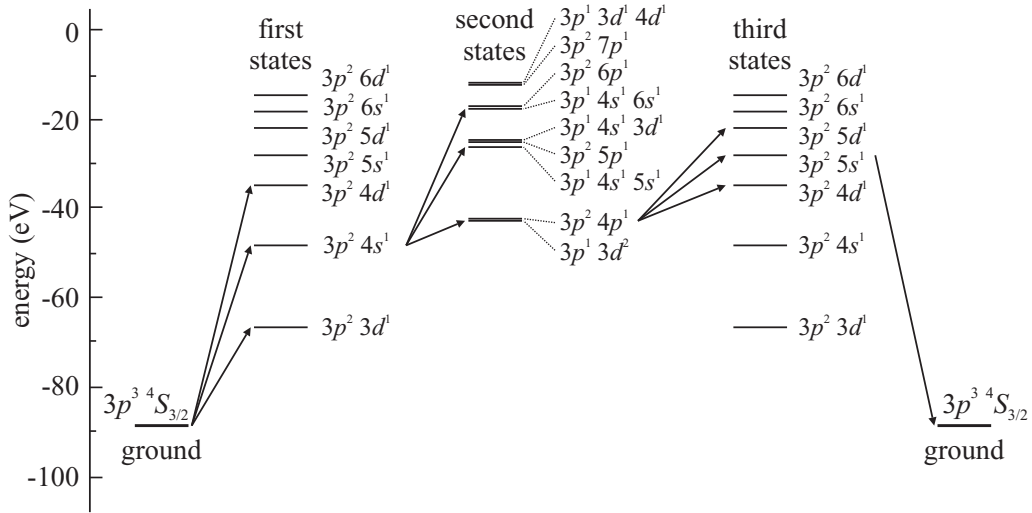


FIG. 3. Energy diagram of  $\text{Ar}^{3+}$  ion. The ground state is  $3p^3 \ ^4S_{3/2}$ . The fine structures of the excited states are not shown but are included in our calculation.

within the  $\pm 2\Delta\omega$  spectral range:

$$\omega_{\text{NIR},p} = \omega_{\text{NIR},c} + \left(\frac{p}{2}\right)\Delta\omega_{\text{NIR}}, \quad (18)$$

$$\omega_{\text{EUV},q} = \omega_{\text{EUV},c} + \left(\frac{q}{2}\right)\Delta\omega_{\text{NIR}}, \quad (19)$$

where  $p$  and  $q$  are  $-4, -3, \dots, 3, 4$ . Then we calculate the third-order nonlinear polarizabilities for all possible angular frequency combinations

$$\alpha^{(3)}(p,q) = \alpha^{(3)}(\omega_{\text{NIR},p}, \omega_{\text{EUV},q}, 2\omega_{\text{NIR},p} + \omega_{\text{EUV},q}). \quad (20)$$

After that, we take a weighted average of them to get the final polarizability used in Eq. (12):

$$\alpha_{\text{ave}}^{(3)} = \sum_{p,q} f(p,q) \alpha^{(3)}(p,q) = 3.98 \times 10^{-62} \frac{\text{C m}^4}{\text{V}^3}, \quad (21)$$

where the weighting factor  $f(p,q)$  is proportional to the fractional contribution of each frequency combination to the final output field:

$$f(p,q) = \frac{\tilde{E}_{\text{NIR}}(\omega_{\text{NIR},p})^2 \tilde{E}_{\text{EUV}}(\omega_{\text{EUV},q})}{\sum_{p,q} \tilde{E}_{\text{NIR}}(\omega_{\text{NIR},p})^2 \tilde{E}_{\text{EUV}}(\omega_{\text{EUV},q})}. \quad (22)$$

With broadband input spectra some frequency components may hit a resonance. This can result in large polarizability and strong absorption. However, since the resonant bandwidth

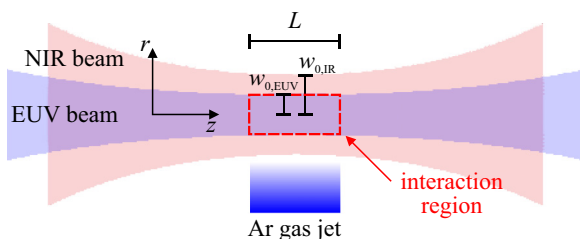


FIG. 4. Configuration of the EUV beam, NIR beam, and the Ar gas jet for a practical four-wave-mixing experiment.

is  $\sim 10^7$ – $10^{11}$  Hz, much smaller than the input bandwidth, the modification of the spectrum within such a small bandwidth can only result in a low and long pedestal of 10 ps to 100 ns in the output pulse. This low and long pedestal can be considered as background interference, which is not part of the physics in the femtosecond timescale that we are interested in.

As shown in Fig. 4, the interaction region is enclosed by the EUV beam radius ( $0 \leq r \leq w_{0,\text{EUV}}$ ) and the gas jet length ( $0 \leq z \leq L$ ), where  $L$  is fixed at 2 mm. Because the interaction length  $L$  is much shorter than the confocal parameters of the NIR beam (24.8 mm) and the EUV beam (105.6 mm), the variations of the beam sizes within the interaction region can be neglected. To simplify the evaluate of the absolute FWM

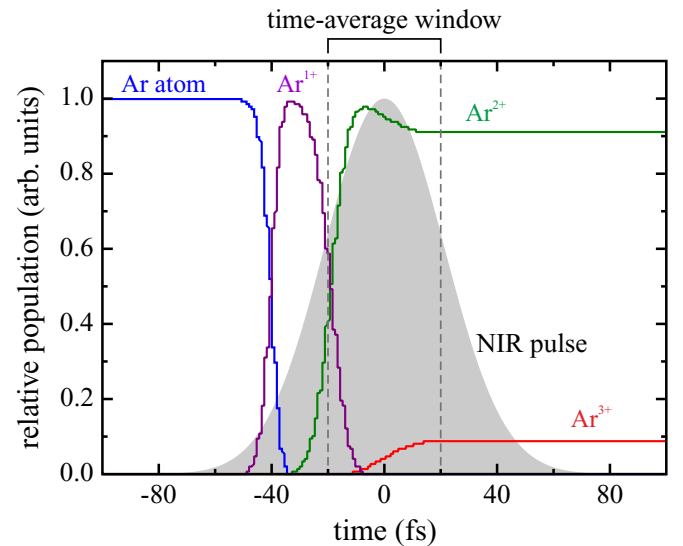


FIG. 5. Relative populations of Ar (blue line),  $\text{Ar}^{1+}$  (purple line),  $\text{Ar}^{2+}$  (green line),  $\text{Ar}^{3+}$  (red line), and the space-averaged NIR intensity distribution  $\bar{I}_{\text{NIR}}(t)$  (gray area) as functions of time. These relative populations are calculated by ADK theory [33]. The dashed lines mark the time-averaged window  $[-\tau_{\text{EUV}}, \tau_{\text{EUV}}]$ .

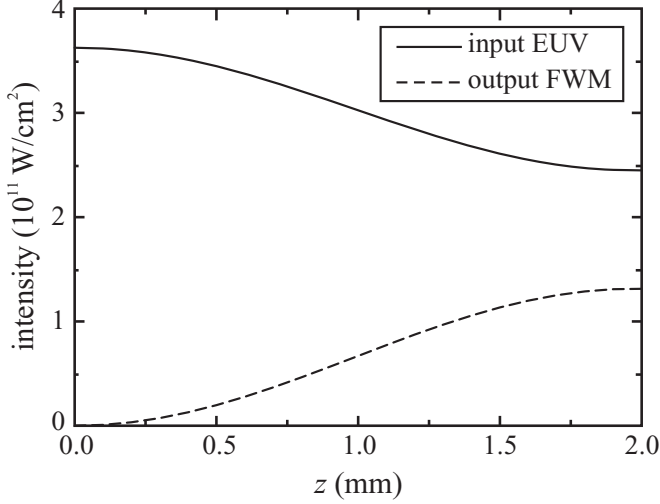


FIG. 6. Calculated input EUV intensity  $I_{\text{EUV}}(z)$  (solid line) and output FWM intensity  $I_{\text{out}}(z)$  (dashed line) as functions of propagation distance  $z$ .

yield, we take the average of the transverse spatial intensity profile of the NIR pulse within the interaction region:

$$\begin{aligned} \bar{I}_{\text{NIR}}(t) &= \frac{1}{\pi w_{0,\text{EUV}}^2} \int_0^{w_{0,\text{EUV}}} I_{\text{NIR}}(r,t) 2\pi r dr \\ &= \bar{I}_{\text{NIR,peak}} \exp\left(-\frac{t^2}{\tau_{\text{NIR}}^2}\right), \end{aligned} \quad (23)$$

where  $\bar{I}_{\text{NIR,peak}} = 2.4 \times 10^{15} \text{ W/cm}^2$  is the spatially averaged peak intensity of the NIR pulse. The spatially averaged temporal intensity profile is used to calculate the populations of Ar ion species by applying the Ammosov-Delone-Krainov (ADK) tunneling ionization theory [33]. The results are shown in Fig. 5. It can be seen that the Ar atoms are well-ionized to the designed ionization stage  $\text{Ar}^{2+}$  before the pulse peak arrives. The time average of the relative  $\text{Ar}^{2+}$  and electron populations within the EUV pulse duration ( $-\tau_{\text{EUV}} \leq t \leq \tau_{\text{EUV}}$ ) reach  $\eta_{\text{ion}} = 0.89$  and  $\eta_e = 1.98$ , respectively.

In order to use Eq. (12) to evaluate the FWM output at 42.6 nm, we calculate the space-time-averaged intensities of the input NIR and EUV fields within the interaction region and EUV pulse duration:

$$\hat{I}_{\text{NIR}} = \frac{1}{2\tau_{\text{EUV}}} \int_{-\tau_{\text{EUV}}}^{\tau_{\text{EUV}}} \bar{I}_{\text{NIR}}(t) dt = 2.1 \times 10^{15} \text{ W/cm}^2 \quad (24)$$

and

$$\begin{aligned} \hat{I}_{\text{EUV}} &= \frac{1}{2\tau_{\text{EUV}}} \int_{-\tau_{\text{EUV}}}^{\tau_{\text{EUV}}} \left[ \frac{1}{\pi w_{0,\text{EUV}}^2} \int_0^{w_{0,\text{EUV}}} I_{\text{EUV}}(r,t) 2\pi r dr \right] dt \\ &= 3.6 \times 10^{11} \text{ W/cm}^2, \end{aligned} \quad (25)$$

respectively. These two space-time-averaged intensities serve as the initial condition of Eq. (12).

Finally, the input EUV intensity and output FWM intensity as functions of propagation distance  $z$  are obtained by Eq. (12). The results are shown in Fig. 6. The atom density  $N_{\text{atom}} = 1.35 \times 10^{17} \text{ cm}^{-3}$  is chosen to match the dephasing length ( $L_d = \pi/\Delta k$ ) with the interaction length  $L$ . Therefore, the

output FWM intensity reaches maximum at the end of the gas jet:

$$I_{\text{out}}(L) = 1.31 \times 10^{11} \text{ W/cm}^2. \quad (26)$$

With the assumption that the output FWM field has the same beam radius and pulse duration of the input EUV field, the output FWM energy is obtained:

$$U_{\text{out}} = I_{\text{out}}(L) \times \pi w_{0,\text{EUV}}^2 \times 2\tau_{\text{EUV}} = 264 \text{ nJ}, \quad (27)$$

corresponding to an EUV-to-EUV conversion efficiency of 26%.

In the proposed condition, the electron density is so low ( $N_e = \eta_e N_{\text{atom}} = 2.68 \times 10^{17} \text{ cm}^{-3}$ ) that the group-delay dispersions (GDD) for the input NIR and EUV pulses are only  $-0.5 \text{ fs}^2$  and  $-9.4 \times 10^{-5} \text{ fs}^2$ , respectively. Therefore, the influence of GDD on NIR and EUV pulse durations is negligible. The group-velocity mismatch between the NIR and EUV pulses is also small. The time difference between the EUV and NIR pulses after passing through the 2 mm plasma is only about 0.6 fs. Comparing to their pulse durations, the walk-off effect can also be neglected. By applying the ionization rate calculated by the ADK theory, the variation of electron density is obtained. Then the spectrum shifts due to strong self-phase modulation are estimated to be about  $2.0 \times 10^{13}$  and  $1.2 \times 10^{12} \text{ Hz}$  for the NIR and EUV pulses, respectively [57]. Such angular frequency shifts are smaller than the initial bandwidths of the NIR and EUV pulses. Therefore, the effect of ionization spectrum shifts is already included in the weighted average of the nonlinear polarizability. The parameters used in our calculation are summarized in Table III.

The case of EUV four-wave mixing described above operates in a condition with low material density but high electric field, which is different from the traditional nonlinear optical process using nonlinear crystals. To show the differences, we compare with the NIR cross-polarized-wave (XPW) generation in  $\text{BaF}_2$  crystal [58,59]. This is also a third-order nonlinear process, which is used for temporal contrast enhancement of ultrashort laser pulses [60,61]. The comparison of these two processes is shown in Table IV.

It can be seen that the nonlinear polarizabilities of a  $\text{BaF}_2$  cell and an  $\text{Ar}^{2+}$  ion have the same order of magnitude. However, the applied electric field on  $\text{BaF}_2$  for XPW is limited by its damage threshold, which is much smaller than the NIR field applied on  $\text{Ar}^{2+}$  for EUV FWM. This shows the advantage of using ions as the interacting medium since a

TABLE III. Parameters used in the NIR-EUV four-wave-mixing calculation.

	Input NIR field	Input EUV field
Wavelength	810 nm	47.6 nm
Beam waist radius	80 $\mu\text{m}$	40 $\mu\text{m}$
Pulse duration	30 fs	20 fs
Input pulse energy	16.5 mJ	1 $\mu\text{J}$
Space-time-averaged Intensity	$2.1 \times 10^{15} \text{ W/cm}^2$	$3.6 \times 10^{11} \text{ W/cm}^2$
	Ar atom	$\text{Ar}^{2+}$
Average density	$1.35 \times 10^{17} \text{ cm}^{-3}$	$1.21 \times 10^{17} \text{ cm}^{-3}$

TABLE IV. Comparison of NIR XPW generation and EUV four-wave mixing.

	NIR XPW by BaF <sub>2</sub> [59]	EUV FWM by Ar <sup>2+</sup>
Density $N$ (cm <sup>-3</sup> )	$1.68 \times 10^{22}$	$1.21 \times 10^{17}$
Nonlinear polarizability $\alpha^{(3)}$ (C-m <sup>4</sup> /V <sup>3</sup> )	$8.38 \times 10^{-62}$	$3.98 \times 10^{-62}$
Nonlinear susceptibility $\chi^{(3)}$ (m <sup>2</sup> /V <sup>2</sup> )	$1.59 \times 10^{-22}$	$5.44 \times 10^{-28}$
Operation electric field (V/m)	$E = 2.75 \times 10^9$	$E_{\text{NIR}} = 8.89 \times 10^{10}$ $E_{\text{EUV}} = 1.17 \times 10^9$
Induced nonlinear dipole moment (C-m)	$p^{(3)} = \alpha^{(3)} E^3$ $= 1.73 \times 10^{-33}$	$p^{(3)} = \alpha^{(3)} E_{\text{EUV}} E_{\text{NIR}}^2$ $= 3.67 \times 10^{-31}$
Induced nonlinear polarization (C/m <sup>-2</sup> )	$P^{(3)} = \epsilon_0 \chi^{(3)} E^3$ $= 2.91 \times 10^{-5}$	$P^{(3)} = \epsilon_0 \chi^{(3)} E_{\text{EUV}} E_{\text{NIR}}^2$ $= 4.44 \times 10^{-8}$
Input pulse energy	$U_{\text{in}} = 1.2$ mJ	$U_{\text{NIR}} = 16.5$ mJ $U_{\text{EUV}} = 1$ $\mu$ J
Output energy	$U_{\text{out}} = 0.12$ mJ	$U_{\text{out}} = 264$ nJ From NIR to FWM : $\eta_{\text{NIR}} = 1.6 \times 10^{-5}$
Conversion efficiency	$\eta_{\text{XPW}} = 10\%$	From EUV to FWM : $\eta_{\text{EUV}} = 26\%$

much higher electric field can be used. In this case the induced nonlinear dipole moment of an Ar<sup>2+</sup> ion is two orders of magnitude larger than that on a BaF<sub>2</sub> cell. However, the Ar<sup>2+</sup> density is much smaller than the BaF<sub>2</sub> density. Therefore, the induced nonlinear polarization on Ar<sup>2+</sup> plasma for EUV FWM is still three orders of magnitude smaller than that on BaF<sub>2</sub> crystal for NIR XPW. This is why the energy depletion of the NIR pulse is negligible. Yet, from the point of view of EUV-to-EUV conversion, the FWM process acts as an amplification process for the output EUV wave. The conver-

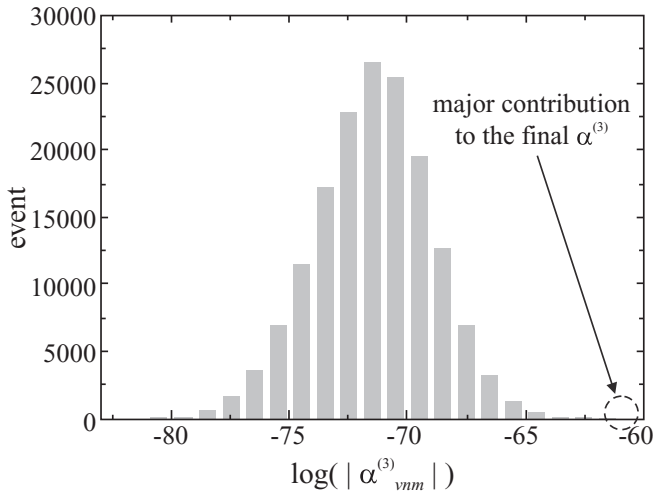


FIG. 7. Distribution of the absolute values of the contributed third-order nonlinear polarizability  $\alpha_{vnm}^{(3)}$  of each transition calculated in Sec. II, for the four-wave mixing of 1 EUV photon (47.6 nm) plus two NIR photons (810 nm) to a second EUV photon (42.6 nm). Due to the fact that these  $|\alpha_{vnm}^{(3)}|$  spread to a large range, the histogram is plotted with the log of  $|\alpha_{vnm}^{(3)}|$ . The major contribution to the final  $\alpha^{(3)}$  is marked in the dashed circle.

sion efficiency can reach  $\eta_{\text{EUV}} = 26\%$  due to the large NIR field.

In Eq. (5) there is an implicit assumption that fifth-order nonlinearity and above can be neglected. If not, higher-order terms should be included in the coupled wave equations. To verify this assumption, we plot the distribution of the absolute values of  $\alpha_{vnm}^{(3)}$  [Eq. (2)] in Fig. 7. It can be seen that these  $|\alpha_{vnm}^{(3)}|$  span a large range (from  $10^{-82}$  to  $10^{-61}$  C m<sup>4</sup>/V<sup>3</sup>). The major contribution to  $\alpha^{(3)}$  comes from only a few near-resonant transitions. Therefore, we can estimate the higher-order nonlinear polarizability by considering just the near-resonant transitions. The estimated value of the fifth-order nonlinear polarizability for the wave mixing of 1 EUV photon (47.6 nm) plus 4 NIR photons (810 nm) to a second EUV photon is about  $10^{-85}$  C m<sup>6</sup>/V<sup>5</sup>. For the case under consideration, the resulted fifth-order nonlinear dipole moment in an Ar<sup>2+</sup> ion is about  $10^{-33}$  C m, which is less than 1% of the third-order nonlinear dipole moment. Higher-order nonlinearity can indeed be neglected in our calculations.

## V. CONCLUSION AND PROSPECTS

We have analyzed a nonlinear wave-mixing process of EUV and NIR waves using rare gas ions as the interacting medium and discussed its applications in EUV optics. The third-order nonlinear polarizabilities of Ar<sup>2+</sup> and Ar<sup>3+</sup> ions for the four-wave mixing of one EUV photon plus two NIR photons to a second EUV photon are calculated using Cowan's atomic structure code and the Wigner-Eckart theorem. The FWM yield is derived and a practical experimental configuration with microjoule EUV pulse and millijoule NIR pulse mixed in an Ar gas jet is studied. The expected EUV-to-EUV conversion efficiency reaches 26%.

The process can be used for EUV frequency conversion. It is well known that EUV or x-ray lasers [4–7] can generate intense EUV or x-ray pulses at specific wavelengths with a narrow line width. They are useful for EUV or x-ray microscopy [62,63], holography [64,65], and interferometry of high-density plasmas [66,67]. However, because the wavelengths are fixed by atomic energy levels, EUV or x-ray lasers cannot be tuned continuously for spectroscopic applications. By using the FWM technique, EUV frequency conversion can be achieved with high efficiency, which may greatly extend the versatility and flexibility of EUV or x-ray lasers.

The FWM technique can also be utilize for single-shot, EUV waveform measurement. The output FWM field is proportional to the input EUV field times the square of the NIR field:

$$E_{\text{out}} \propto E_{\text{EUV}} E_{\text{NIR}}^2. \quad (28)$$

The NIR field can be characterized in advance by using well-developed techniques such as frequency-resolved optical gating (FROG) [40,68], spectral interferometry for direct electric field reconstruction (SPIDER) [39,69], or modified interferometric field autocorrelation (MIFA) [41]. The NIR pulse serves as the gate pulse acting on the unknown EUV field, thus the output FWM field is equivalent to the signal of a cross-correlation FROG (XFROG) [48]. By crossing the EUV beam and NIR beam with a small angle on the Ar gas jet, a sweep of NIR gate pulse arrival time is encoded across the EUV beam profile. Then, by using an imaging spectrometer to



record the power spectrum of the FWM field as a function of the gate pulse arrival time, the XFROG trace can be obtained in one shot:

$$I_{\text{XFROG}}(\omega, \tau) \propto \left| \int_{-\infty}^{\infty} E_{\text{EUV}}(t) E_{\text{NIR}}(t - \tau)^2 e^{i\omega t} dt \right|^2. \quad (29)$$

Then the EUV waveform  $E_{\text{EUV}}(t)$  can be retrieved by using the XFROG iteration algorithm [48] or by functional differentiation [47] where the trial function for the unknown field can be obtained directly from the functional derivative of the error function. The latter method is not only fast and reliable but also ensures the uniqueness of the solution. This will be an all-optical method for single-shot measurement of EUV waveform that to our knowledge has not been developed before.

The EUV-NIR FWM process can also be used for EUV waveform control. Since NIR waveform programming methods have been well developed [38,49] and commercial apparatuses for this purpose are available [70], a preprogrammed NIR waveform can be used to control the output EUV field as shown in Eq. (28).

In view of its efficiency and potential applications, we believe EUV-NIR FWM using ion plasmas as the nonlinear media is a promising new direction to explore for the advancement of EUV optics.

#### ACKNOWLEDGMENTS

This work was supported by the research projects funded by the Ministry of Science and Technology, Taiwan under Grants No. MOST-106-2112-M-008-018 and No. MOST-105-2112-M-001-005-MY3.

- 
- [1] P. B. Corkum and F. Krausz, *Nat. Phys.* **3**, 381 (2007).  
 [2] C. Winterfeldt, C. Spielmann, and G. Gerber, *Rev. Mod. Phys.* **80**, 117 (2008).  
 [3] T. Popmintchev, M.-C. Chen, P. Arpin, M. M. Murnane, and H. C. Kapteyn, *Nat. Photonics* **4**, 822 (2010).  
 [4] H. Daido, *Rep. Prog. Phys.* **65**, 1513 (2002).  
 [5] P. Zeitoun, G. Faivre, S. Sebban, T. Mocek, A. Hallou, M. Fajardo, D. Aubert, P. Balcou, F. Burgy, D. Douillet, S. Kazamias, G. de Lachèze-Murel, T. Lefrou, S. le Pape, P. Mercère, H. Merdji, A. S. Morlens, J. P. Rousseau, and C. Valentin, *Nature (London)* **431**, 426 (2004).  
 [6] M.-C. Chou, P.-H. Lin, C.-A. Lin, J.-Y. Lin, J. Wang, and S.-Y. Chen, *Phys. Rev. Lett.* **99**, 063904 (2007).  
 [7] S. Suckewer and P. Jaeglé, *Laser Phys. Lett.* **6**, 411 (2009).  
 [8] B. W. J. McNeil and N. R. Thompson, *Nat. Photonics* **4**, 814 (2010).  
 [9] P. R. Ribic and G. Margaritondo, *J. Phys. D* **45**, 213001 (2012).  
 [10] C. Bostedt, S. Boutet, D. M. Fritz, Z. Huang, H. J. Lee, H. T. Lemke, A. Robert, W. F. Schlotter, J. J. Turner, and G. J. Williams, *Rev. Mod. Phys.* **88**, 015007 (2016).  
 [11] S. Hüfner, *Photoelectron Spectroscopy*, 3rd ed. (Springer, New York, 2003).  
 [12] M.-C. Chou, R.-P. Huang, P.-H. Lin, C.-T. Huang, S.-Y. Chen, H.-H. Chu, J. Wang, and J.-Y. Lin, *Opt. Lett.* **34**, 623 (2009).  
 [13] M. K. Kim, *J. Photonics Energy* **1**, 018005 (2010).  
 [14] M. Bauer, *J. Phys. D* **38**, R253 (2005).  
 [15] H. N. Chapman, A. Barty, M. J. Bogan, S. Boutet, M. Frank, S. P. Hau-Riege, S. Marchesini, B. W. Woods, S. carona Bajt, W. H. Benner, R. A. London, E. Plnjes, M. Kuhlmann, R. Treusch, S. Dsterer, T. Tschentscher, J. R. Schneider, E. Spiller, T. Mller, C. Bostedt, M. Hoener, D. A. Shapiro, K. O. Hodgson, D. van der Spoel, F. Burmeister, M. Bergh, C. Caleman, G. Huld, M. M. Seibert, F. R. N. C. Maia, R. W. Lee, A. Szöke, N. Timneanu, and J. Hajdu, *Nat. Phys.* **2**, 839 (2006).  
 [16] E. B. Malm, N. C. Monserud, C. G. Brown, P. W. Wachulak, H. Xu, G. Balakrishnan, W. Chao, E. Anderson, and M. C. Marconi, *Opt. Express* **21**, 9959 (2013).  
 [17] F. Krausz and M. Ivanov, *Rev. Mod. Phys.* **81**, 163 (2009).  
 [18] L. Gallmann, C. Cirelli, and U. Keller, *Annu. Rev. Phys. Chem.* **63**, 447 (2012).  
 [19] A. Melnikov, H. Prima-Garcia, M. Lisowski, T. Gießel, R. Weber, R. Schmidt, C. Gahl, N. M. Bulgakova, U. Bovensiepen, and M. Weinelt, *Phys. Rev. Lett.* **100**, 107202 (2008).  
 [20] C. La-O-Vorakiat, M. Siemens, M. M. Murnane, H. C. Kapteyn, S. Mathias, M. Aeschlimann, P. Grychtol, R. Adam, C. M. Schneider, J. M. Shaw, H. Nembach, and T. J. Silva, *Phys. Rev. Lett.* **103**, 257402 (2009).  
 [21] S. Mukamel, D. Abramavicius, L. Yang, W. Zhuang, I. V. Schweigert, and D. V. Voronine, *Acc. Chem. Res.* **42**, 553 (2009).  
 [22] A. H. Kung, J. F. Young, G. C. Bjorklund, and S. E. Harris, *Phys. Rev. Lett.* **29**, 985 (1972).  
 [23] J. Reintjes, *Appl. Opt.* **19**, 3889 (1980).  
 [24] J. F. Reintjes, *Nonlinear Optical Parametric Processes in Liquids and Gases* (Academic Press, San Diego, 1984).  
 [25] K. Boyer, H. Egger, T. S. Luk, H. Pummer, and C. K. Rhodes, *J. Opt. Soc. Am. B* **1**, 3 (1984).  
 [26] G. Hilber, A. Lago, and R. Wallenstein, *J. Opt. Soc. Am. B* **4**, 1753 (1987).  
 [27] A. McPherson, G. Gibson, H. Jara, U. Johann, T. S. Luk, I. A. McIntyre, K. Boyer, and C. K. Rhodes, *J. Opt. Soc. Am. B* **4**, 595 (1987).  
 [28] J. P. Marangos, N. Shen, H. Ma, M. H. R. Hutchinson, and J. P. Connerade, *J. Opt. Soc. Am. B* **7**, 1254 (1990).  
 [29] S. Hannemann, U. Hollenstein, E.-J. van Duijn, and W. Ubachs, *Opt. Lett.* **30**, 1494 (2005).  
 [30] W. Cao, E. R. Warrick, A. Fidler, S. R. Leone, and D. M. Neumark, *Phys. Rev. A* **94**, 021802 (2016).  
 [31] W. Cao, E. R. Warrick, A. Fidler, D. M. Neumark, and S. R. Leone, *Phys. Rev. A* **94**, 053846 (2016).  
 [32] F. Bencivenga, R. Cucini, F. Capotondi, A. Battistoni, R. Mincigrucci, E. Giangrisostomi, A. Gessini, M. Manfredda, I. P. Nikolov, E. Pedersoli, E. Principi, C. Svetina, P. Parisse, F. Casolari, M. B. Danailov, M. Kiskinova, and C. Masciovecchio, *Nature (London)* **520**, 205 (2015).  
 [33] M. V. Ammosov, N. B. Delone, and V. P. Krainov, *Zh. Eksp. Teor. Fiz.* **91**, 2008 (1986) [*J. Exp. Theor. Phys.* **64**, 1191 (1986)].

- [34] B. Sheehy and L. F. DiMauro, *Annu. Rev. Phys. Chem.* **47**, 463 (1996).
- [35] S. V. Popruzhenko, *J. Phys. B: At. Mol. Opt. Phys.* **47**, 204001 (2014).
- [36] R. D. Cowan, *The Theory of Atomic Structure and Spectra* (University of California Press, Berkeley, 1981), pp. 12–15.
- [37] A. M. Weiner, J. P. Heritage, and E. M. Kirschner, *J. Opt. Soc. Am. B* **5**, 1563 (1988).
- [38] F. Verluise, V. Laude, Z. Cheng, C. Spielmann, and P. Tournois, *Opt. Lett.* **25**, 575 (2000).
- [39] C. Iaconis and I. A. Walmsley, *Opt. Lett.* **23**, 792 (1998).
- [40] R. Trebino, *Frequency-Resolved Optical Gating: The Measurement of Ultrashort Laser Pulses* (Springer, New York, 2002).
- [41] S.-D. Yang, C.-S. Hsu, S.-L. Lin, H. Miao, C.-B. Huang, and A. M. Weiner, *Opt. Express* **16**, 20617 (2008).
- [42] Y. Mairesse and F. Quéré, *Phys. Rev. A* **71**, 011401 (2005).
- [43] G. Sansone, E. Benedetti, F. Calegari, C. Vozzi, L. Avaldi, R. Flammini, L. Poletto, P. Villoresi, C. Altucci, R. Velotta, S. Stagira, S. De Silvestri, and M. Nisoli, *Science* **314**, 443 (2006).
- [44] P. M. Paul, E. S. Toma, P. Breger, G. Mullot, F. Aug, P. Balcou, H. G. Muller, and P. Agostini, *Science* **292**, 1689 (2001).
- [45] H. G. Muller, *Appl. Phys. B* **74**, s17 (2002).
- [46] H. Hsin Chu, C.-H. Yang, S.-C. Liu, and J. Wang, *Opt. Express* **23**, 34082 (2015).
- [47] T.-W. Yau, C.-H. Lee, and J. Wang, *J. Opt. Soc. Am. B* **17**, 1626 (2000).
- [48] S. Linden, J. Kuhl, and H. Giessen, *Opt. Lett.* **24**, 569 (1999).
- [49] H.-S. Chan, Z.-M. Hsieh, W.-H. Liang, A. H. Kung, C.-K. Lee, C.-J. Lai, R.-P. Pan, and L.-H. Peng, *Science* **331**, 1165 (2011).
- [50] R. W. Boyd, *Nonlinear Optics* (Academic Press, San Diego, 1992).
- [51] R. D. Cowan, *The Theory of Atomic Structure and Spectra*, (University of California Press, Berkeley, 1981), p. 305.
- [52] T.-S. Hung, C.-H. Yang, J. Wang, S.-Y. Chen, J.-Y. Lin, and H.-H. Chu, *Appl. Phys. B* **117**, 1189 (2014).
- [53] M. Lewenstein, K. C. Kulander, K. J. Schafer, and P. H. Bucksbaum, *Phys. Rev. A* **51**, 1495 (1995).
- [54] E. Takahashi, Y. Nabekawa, and K. Midorikawa, *Opt. Lett.* **27**, 1920 (2002).
- [55] J.-F. Hergott, M. Kovacev, H. Merdji, C. Hubert, Y. Mairesse, E. Jean, P. Breger, P. Agostini, B. Carré, and P. Salières, *Phys. Rev. A* **66**, 021801 (2002).
- [56] I. J. Kima, G. H. Lee, S. B. Park, Y. S. Lee, T. K. Kim, and C. H. Nam, *Appl. Phys. Lett.* **92**, 021125 (2008).
- [57] S. C. Rae and K. Burnett, *Phys. Rev. A* **46**, 1084 (1992).
- [58] N. Minkovski, S. M. Saltiel, G. I. Petrov, O. Albert, and J. Etchepare, *Opt. Lett.* **27**, 2025 (2002).
- [59] N. Minkovski, G. I. Petrov, S. M. Saltiel, O. Albert, and J. Etchepare, *J. Opt. Soc. Am. B* **21**, 1659 (2004).
- [60] A. Jullien, O. Albert, F. Burgy, G. Hamoniaux, J.-P. Rousseau, J.-P. Chambaret, F. Augé-Rochereau, G. Chériaux, J. Etchepare, N. Minkovski, and S. M. Saltiel, *Opt. Lett.* **30**, 920 (2005).
- [61] V. Chvykov, P. Rousseau, S. Reed, G. Kalinchenko, and V. Yanovsky, *Opt. Lett.* **31**, 1456 (2006).
- [62] S. Suckewer and C. Skinner, *Science* **247**, 1553 (1990).
- [63] C. A. Brewer, F. Brizuela, P. Wachulak, D. H. Martz, W. Chao, E. H. Anderson, D. T. Attwood, A. V. Vinogradov, I. A. Artyukov, A. G. Ponomareko, V. V. Kondratenko, M. C. Marconi, J. J. Rocca, and C. S. Menoni, *Opt. Lett.* **33**, 518 (2008).
- [64] J. E. Trebes, S. B. Brown, E. M. Campbell, D. L. Matthews, D. G. Nilson, G. F. Stone, and D. A. Whelan, *Science* **238**, 517 (1987).
- [65] H. Daido, M. S. Schulz, K. Murai, R. Kodama, G. Yuan, J. Goto, K. A. Tanaka, Y. Kato, S. Nakai, K. Shinohara, T. Honda, I. Kodama, H. Iwasaki, T. Yoshinobu, M. Tsukamoto, M. Niibe, Y. Fukuda, D. Neely, A. Macphee, and G. Slark, *J. X-ray Sci. Technol.* **5**, 105 (1995).
- [66] L. B. Da Silva, T. W. Barbee, Jr., R. Cauble, P. Celliers, D. Ciarlo, S. Libby, R. A. London, D. Matthews, S. Mrowka, J. C. Moreno, D. Ress, J. E. Trebes, A. S. Wan, and F. Weber, *Phys. Rev. Lett.* **74**, 3991 (1995).
- [67] R. F. Smith, J. Dunn, J. Nilsen, V. N. Shlyaptsev, S. Moon, J. Filevich, J. J. Rocca, M. C. Marconi, J. R. Hunter, and T. W. Barbee, *Phys. Rev. Lett.* **89**, 065004 (2002).
- [68] R. Trebino and D. J. Kane, *J. Opt. Soc. Am. A* **10**, 1101 (1993).
- [69] C. Iaconis and I. A. Walmsley, *IEEE J. Quantum Electron.* **35**, 501 (1999).
- [70] Dazzler, Fastlite Inc., <http://www.fastlite.com>.